10th IFAC Symposium on Robot Control
International Federation of Automatic Control
September 5-7, 2012. Dubrovnik, Croatia

IFAC

Vision-Based Loitering Over a Target for a Fixed-Wing UAV

**Pietro Peliti   Lorenzo Rosa   Giuseppe Oriolo
Marilena Vendittelli**

*Dipartimento di Ingegneria Informatica, Automatica e Gestionale,
Università di Roma La Sapienza, via Ariosto 25, 00185, Roma, Italy
(e-mail: {peliti,rosa,oriolo,vendittelli}@dis.uniroma1.it)*

Abstract: For a fixed-wing Unmanned Aerial Vehicle (UAV) equipped with a gimbaled camera, we consider the problem of tracking a visual target while simultaneously bringing the UAV to orbit on a circular trajectory centered above the target. To achieve this kind of loitering behavior, we propose a feedback control method that is inspired by image-based visual servoing and makes use of a backstepping technique. Through this approach, we are able to obtain a control law that requires only image and proprioceptive data. A formal proof of convergence and a set of validating numerical trials are provided, including a realistic simulation on a commercial UAV.

Keywords: UAV, feedback control, visual servoing, target tracking, backstepping

1. INTRODUCTION

Unmanned Aerial Vehicles (UAVs) are increasingly used in many applications including environment monitoring, search and rescue, surveillance, patrolling, and escorting. However, improving the autonomy of these systems is still a scientific challenge. Different kinds of UAVs are commercially available or have been designed for research purposes. They may differ in size, shape and actuation, resulting in different flight characteristics, but the sensing equipment invariably includes an Inertial Measurement Unit (IMU) and a camera. Fixed-wing UAVs are of particular interest when efficiency and endurance is a concern.

A typical task for a UAV is the continued observation of a ground target, either selected by a remote human operator or automatically identified by the UAV itself. While a VTOL UAV can conveniently accomplish this by hovering above the target (Bourquardez et al., 2009), a fixed-wing UAV requires non-zero airspeed to fly and therefore must loiter along a suitable trajectory.

In principle, one way to achieve loitering is to define a reference trajectory for the UAV in ground coordinates. This can be done if the position of the UAV and the relative position of the target w.r.t. the UAV are available. The first may be provided by a Global Positioning System (GPS) while the second can be reconstructed fusing visual and inertial data; in an escorting mission, or whenever it is collaborative, the target may even directly communicate its ground position to the UAV. Methods that can be classified in this category were proposed by Stolle and Rysdyk (2003) and Quigleyand et al. (2005) .

In certain operative conditions, however, it may be preferable to adopt the visual servoing paradigm to design control schemes that rely on image and proprioceptive data only (Chaumette and Hutchinson, 2006). This approach is computationally simpler and can be expected to provide a more reactive behavior, e.g., if the target is moving. Moreover, it does not need GPS data, which may be unreliable or even unavailable, temporarily or permanently.

Visual servoing methods can be classified as either position-based (PBVS) or image-based (IBVS). Using PBVS for loitering requires an estimate of the relative pose of the target with respect to the UAV. Tools like the Extended Kalman Filter can be used to robustly estimate this information (Watanabe et al., 2009). Ma et al. (2010) and Theodorakopoulos and Lacroix (2008) presented PBVS strategies that use polar rather than cartesian coordinates and a visual measurement of the bearing angle between the target and the UAV. It is well known, however, that PBVS is sensitive to kinematic model errors, imprecise camera calibration and image noise.

IBVS methods are a more robust alternative. For example, Chen and Dawson (2006) proposed an IBVS control strategy for the related problem of tracking a moving UAV. In the work of Le Bras et al. (2009), a control scheme based on spherical projection and optic flow is developed for the case of a UAV equipped with a fixed camera; convergence to a circular trajectory is enforced by a suitable definition of the visual task.

In this paper, we consider a fixed-wing UAV equipped with a *gimbaled* camera flying above a target; our objective is to lead the UAV to orbit on a circular trajectory centered above the target. An advantage of this kind of loitering is to require zero roll rate at steady-state, at least in the absence of wind. Moreover, a circular trajectory allows to monitor the target from every side and is optimal for its localization (Ponda and Frazzoli, 2009).

Our interest in this work is to investigate how circular loitering can be naturally produced by vision-based control laws that do not need inertial coordinate measurements. To this end, we adopt the IBVS approach to design a controller that uses visual and proprioceptive data only.
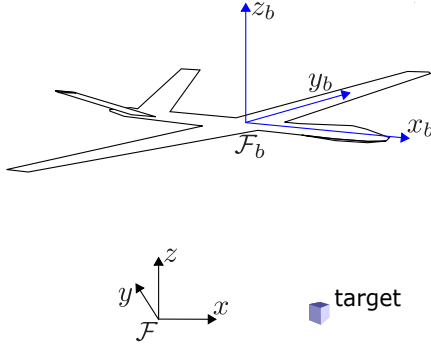
Fig. 1. The UAV body frame $\mathcal{F}_b$ and the ground frame $\mathcal{F}$.
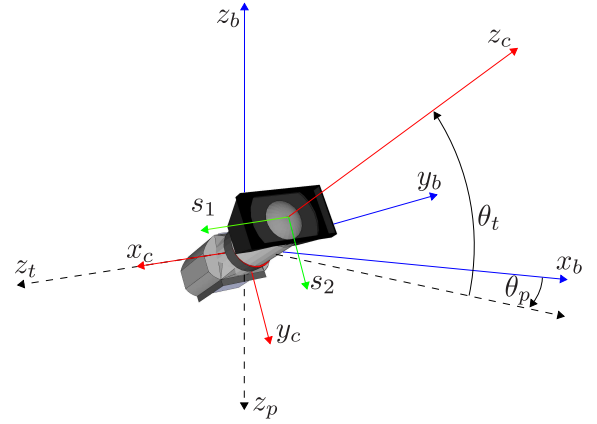

Fig. 2. The gimbaled camera system with the pan and tilt angles (θ_p, θ_t) and the corresponding axes (z_p, z_t). Also shown are the camera frame $\mathcal{F}_c = \{x_c, y_c, z_c\}$ and the image plane coordinates s_1, s_2.

In particular, it is first shown that regulation of the visual features plus the pan angle to a suitable set-point entails convergence to the desired kind of trajectory; then, such regulation is achieved for a simplified model of the UAV+camera system with direct yaw control; finally, the same behavior is obtained for the original UAV+camera system through backstepping. Enhancements to the basic scheme are proposed, including the enforcement of a desired radius for the circular trajectory, a simplified roll control technique, and the integration of an estimator to make sure that the depth of the visual target is not needed for implementation. Simulations are presented for both the ideal UAV dynamics used for design and for a realistic model of a commercial UAV.

The paper is organized as follows. In Sect. 2 a model of the UAV+camera system is introduced, while in Sect. 3 the loitering problem is formulated. Our control method is presented in Sect. 4 and validated through preliminary simulations in Sect. 5. Improvements to the basic scheme are discussed in Sect. 6. Section 7 reports simulation results for the full nonlinear model of an Aerosonde UAV, while Sect. 8 hints at possible future work.

2. MATHEMATICAL MODEL

Consider the fixed-wing UAV in Fig. 1, with the body frame $\mathcal{F}_b$ attached to its center of gravity. Generalized coordinates are the cartesian coordinates (x, y, z) of the origin of $\mathcal{F}_b$ in a ground frame $\mathcal{F}$, plus the orientation of $\mathcal{F}_b$ w.r.t. $\mathcal{F}$, parameterized through the Euler angles ZYX (ψ, θ, ϕ), i.e., the UAV yaw, pitch and roll angles.

The UAV is equipped with a gimbaled camera, i.e., a camera mounted on a pan-tilt mechanism (see Fig. 2). It is assumed that the camera focus coincides with the pan-tilt joint center, and that both are located exactly at the UAV center of gravity. We emphasize that this assumption is only taken for ease of presentation and does not imply any loss of generality; in fact, it is easy to modify all our developments to account for linear/angular offsets between the above three points. The pan-tilt angles θ_p, θ_t complete the generalized coordinates of the UAV+camera system.

Throughout the paper, we denote by s_σ (c_σ) the sine (cosine) of angle σ, by $\boldsymbol{M}_i$ ($\boldsymbol{M}^i$) the i-th column (row) of matrix $\boldsymbol{M}$, and by $\boldsymbol{M}_{i-j}$ ($\boldsymbol{M}^{i-j}$) its submatrix obtained taking columns (rows) $i, i+1, \ldots, j$.

2.1 UAV+camera dynamics

The UAV dynamics of this paper are derived from a general fixed-wing aircraft model under the assumptions that *(i)* there is no wind *(ii)* the aircraft is cruising at constant altitude z and speed v, with pitch, attack and sideslip angles all equal to zero. In these conditions, the velocity of the aircraft is directed along the x_b axis. This kind of horizontal flight can be achieved with an inner Stability Augmentation System (SAS), a common option in modern UAVs (Roskam, 2003).

The resulting model of the UAV+camera system is:

$$
\begin{aligned}
\dot{x} &= v \cos\psi \\
\dot{y} &= v \sin\psi \\
\dot{\psi} &= -\frac{g}{v} \tan\phi \\
\dot{\phi} &= u_\phi \\
\dot{\theta}_p &= u_p \\
\dot{\theta}_t &= u_t
\end{aligned}
\tag{1}
$$

where g is the gravity acceleration. The roll rate u_ϕ, the pan rate u_p and the tilt rate u_t are the available control inputs.

While this is certainly a simplified model, it captures the fundamental complexity of our considered problem. Indeed, the use of equivalent or even simpler models is common when addressing high-level planning and control for UAVs, both in the aerospace and the control/robotics literature; examples include works by Stolle and Rysdyk (2003), Theodorakopoulos and Lacroix (2008), Jung and Tsiotras (2008), Ding et al. (2010), Regina and Zanzi (2011). Note that a more realistic model will be used in the simulation study of Sect. 7 to validate our control design.

2.2 Visual feature kinematics

Consider now a visual point feature associated to the stationary target of interest[1]. Let $\boldsymbol{s} = (s_1 \ s_2)^T$ be the feature coordinates on the image plane x_c, y_c and Z the target depth. The velocity of the feature point is obtained from the velocity $(\boldsymbol{v}_c \ \boldsymbol{\omega}_c)^T$ of the camera in its frame $\mathcal{F}_c$ as

$$\dot{\boldsymbol{s}} = \boldsymbol{J}_i(\boldsymbol{s}, Z) \begin{pmatrix} \boldsymbol{v}_c \\ \boldsymbol{\omega}_c \end{pmatrix}, \qquad (2)$$

where $\boldsymbol{J}_i$ is the so-called interaction matrix (Chaumette and Hutchinson, 2006).

A simple computation shows that the camera velocity is in turn related to the UAV+camera generalized velocities by the relationship

$$\begin{pmatrix} \boldsymbol{v}_c \\ \boldsymbol{\omega}_c \end{pmatrix} = \boldsymbol{J}_c(\psi, \phi, \theta_p, \theta_t) \begin{pmatrix} \dot{x} \\ \dot{y} \\ \dot{\psi} \\ \dot{\phi} \\ \dot{\theta}_p \\ \dot{\theta}_t \end{pmatrix} \qquad (3)$$

in which

$$\boldsymbol{J}_c = \begin{pmatrix} \boldsymbol{R}_{c,1-2} & \boldsymbol{O}_{3\times4} \\ \boldsymbol{O}_{3\times2} & \boldsymbol{R}_c \boldsymbol{\Omega} \end{pmatrix},$$

where $\boldsymbol{R}_c$ is the rotation matrix from $\mathcal{F}$ to $\mathcal{F}_c$ and

$$\boldsymbol{\Omega} = \begin{pmatrix} 0 & c_\psi & -s_\psi s_\phi & s_\psi c_\phi c_{\theta_p} - c_\psi s_{\theta_p} \\ 0 & s_\psi & c_\psi s_\phi & -c_\psi c_\phi c_{\theta_p} - s_\psi s_{\theta_p} \\ 1 & 0 & -c_\phi & -s_\phi c_{\theta_p} \end{pmatrix}.$$

The above expressions are obtained by considering that the UAV vertical velocity $\dot{z}$ and pitch angle θ are both identically zero in the flight condition of interest.

Putting together eqs. (2) and (3), the visual feature kinematics can be written as

$$\dot{\boldsymbol{s}} = \boldsymbol{J}_i(\boldsymbol{s}, Z) \boldsymbol{J}_c(\psi, \phi, \theta_p, \theta_t) \begin{pmatrix} \dot{x} \\ \dot{y} \\ \dot{\psi} \\ \dot{\phi} \\ \dot{\theta}_p \\ \dot{\theta}_t \end{pmatrix}. \qquad (4)$$

3. PROBLEM FORMULATION

Our objective is to devise a control strategy that will move the UAV along a circular trajectory centered above the target and simultaneously keep the observed target at the center of the image. For the reasons discussed in the introduction, we would like to achieve this behavior using visual data provided by the camera and proprioceptive information coming from the UAV inertial navigation system and the pan-tilt joint encoders. We will also assume that a measurement of the UAV speed v is available. In practice, this may be obtained via a Pitot tube, computed from GPS data or reconstructed from optical flow (Le Bras et al., 2009).

---

[1] The important problem of how to choose, extract and track such a feature is outside the scope of this paper; we refer the reader to the pertinent publications in computer vision, such as the one by Drummond and Cipolla (2002).
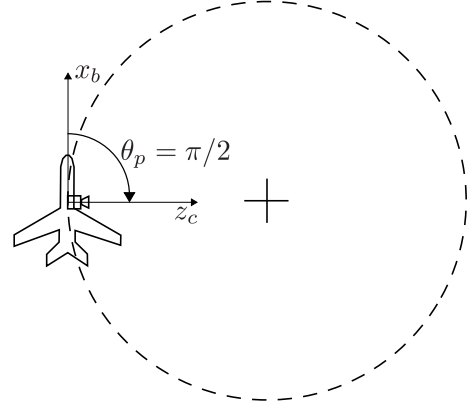

Fig. 3. If the UAV+camera system keeps the target at the center of the image plane and the pan angle θ_p at $\pm\pi/2$, then it is necessarily moving along a circular trajectory centered above the target.

A basic observation is that a purely visual definition of the task is not sufficient to enforce the desired UAV motion. In fact, using the additional degrees of freedom of the pan-tilt platform, the target can be kept at the center of the image (i.e., $\boldsymbol{s} \equiv \boldsymbol{0}$) with the UAV moving along an infinity of trajectories, some of them not even closed. However, this difficulty can be solved by extending the visual task with the value of the pan angle. In fact, simple geometric arguments can be used to prove that the only UAV+camera motion compatible with *maintaining* the set-point $\{\boldsymbol{s} = \boldsymbol{0}, \theta_{\mathbf{p}} = \pm\pi/2\}$ is a clockwise or counterclockwise circular trajectory centered above the target (see Fig. 3). Hence, regulation to this set-point will produce the desired loitering behavior. In addition, the chosen outputs $\boldsymbol{s}$ and θ_p satisfy the requirement of being fully computable from visual or proprioceptive data.

4. CONTROL APPROACH

As stated in the previous section, our objective is now to drive the visual features $\boldsymbol{s}$ to zero and the pan angle θ_p to $\pi/2$ (a clockwise sense of rotation has been chosen). In fact, regulation of these variables will automatically lead the UAV to a circular trajectory. From a control viewpoint, the dynamics of our UAV+camera system are given by eq. (1), with u_ϕ, u_p and u_t as control inputs, while $\boldsymbol{s}$ and θ_p are the output variables.

Since our output vector is actually a simple extension of a visual task, we adopt the classical visual servoing approach based on input-output feedback linearization. This requires the differential map between the outputs and the inputs, which can be derived as follows. Letting

$$\boldsymbol{G}(\psi) = \left(\begin{array}{c|c} \begin{matrix} \cos\psi \\ \sin\psi \end{matrix} & \boldsymbol{O}_{2\times4} \\ \hline \boldsymbol{O}_{4\times1} & \boldsymbol{I}_{4\times4} \end{array} \right),$$

and dropping all dependencies, we can rewrite eq. (4) as

$$\dot{\boldsymbol{s}} = \boldsymbol{J}_i \boldsymbol{J}_c \boldsymbol{G} \begin{pmatrix} v \\ \dot{\psi} \\ \dot{\phi} \\ \dot{\theta}_p \\ \dot{\theta}_t \end{pmatrix} = \boldsymbol{J} \begin{pmatrix} v \\ \dot{\psi} \\ \dot{\phi} \\ \dot{\theta}_p \\ \dot{\theta}_t \end{pmatrix},$$

having set $\boldsymbol{J} = \boldsymbol{J}_i \, \boldsymbol{J}_c \, \boldsymbol{G}$. The above expression can also be written as

$$\dot{\boldsymbol{s}} = \boldsymbol{J}_{1-2} \begin{pmatrix} v \\ \dot{\psi} \end{pmatrix} + \boldsymbol{J}_{3-5} \begin{pmatrix} u_\phi \\ u_p \\ u_t \end{pmatrix}. \qquad (5)$$

The complete input-output differential map is therefore

$$\begin{pmatrix} \dot{\boldsymbol{s}} \\ \dot{\theta}_p \end{pmatrix} = \begin{pmatrix} \boldsymbol{J}_{1-2} \\ 0\ 0 \end{pmatrix} \begin{pmatrix} v \\ \dot{\psi} \end{pmatrix} + \begin{pmatrix} \boldsymbol{J}_{3-5} \\ 0\ 1\ 0 \end{pmatrix} \begin{pmatrix} u_\phi \\ u_p \\ u_t \end{pmatrix}, \qquad (6)$$

which is affine in the control inputs (the first term of the rhs is a *drift*). If the matrix multiplying the input vector (the so-called *decoupling matrix*) were invertible, we could perform feedback linearization to obtain a control law that guarantees exponential convergence of $\boldsymbol{s}$ and θ_p to their set-point. However, one may verify that such matrix is singular exactly at the set-point [2].

In view of the above difficulty, we take a different, two-step approach to design our control law. In the first step, we consider a modified dynamic model which differs from (1) in that it assumes direct, independent control of the yaw angle. A visual control law for this modified system is easily obtained via input-output feedback linearization. In the second step, this control law is used to generate the roll rate u_ϕ for the actual UAV via a backstepping procedure. These two steps are detailed in the following.

4.1 Control of a modified UAV+camera dynamics

Consider the following UAV+camera dynamic model

$$\begin{aligned} \dot{x} &= v \cos\psi \\ \dot{y} &= v \sin\psi \\ \dot{\psi} &= u_\psi \\ \dot{\phi} &= u_\phi \\ \dot{\theta}_p &= u_p \\ \dot{\theta}_t &= u_t. \end{aligned} \qquad (7)$$

This model differs from (1) because the yaw rate is an independent input. To emphasize this, we call this system a *unicycle-like UAV+camera*. Note that the roll rate $\dot{\phi} = u_\phi$ is now assumed to be a known exogenous signal which we cannot manipulate (a disturbance rather than a control).

For the unicycle-like UAV+camera, the expression of the visual feature velocity $\dot{\boldsymbol{s}}$ given by (5) should be reorganized as

$$\dot{\boldsymbol{s}} = (\,\boldsymbol{J}_1\ \boldsymbol{J}_3\,) \begin{pmatrix} v \\ \dot{\phi} \end{pmatrix} + (\,\boldsymbol{J}_2\ \boldsymbol{J}_4\ \boldsymbol{J}_5\,) \begin{pmatrix} u_\psi \\ u_p \\ u_t \end{pmatrix}.$$

The drift term now depends on v and $\dot{\phi}$, rather than $\dot{\psi}$, and the new input vector (with u_ψ in place of u_ϕ) appears in the second term. The complete input-output differential map is therefore given by

$$\begin{pmatrix} \dot{\boldsymbol{s}} \\ \dot{\theta}_p \end{pmatrix} = \begin{pmatrix} \boldsymbol{J}_1\ \boldsymbol{J}_3 \\ 0\quad 0 \end{pmatrix} \begin{pmatrix} v \\ \dot{\phi} \end{pmatrix} + \begin{pmatrix} \boldsymbol{J}_2\ \boldsymbol{J}_4\ \boldsymbol{J}_5 \\ 0\quad 1\quad 0 \end{pmatrix} \begin{pmatrix} u_\psi \\ u_p \\ u_t \end{pmatrix}$$

$$= \boldsymbol{J}_A \begin{pmatrix} v \\ \dot{\phi} \end{pmatrix} + \boldsymbol{J}_B \begin{pmatrix} u_\psi \\ u_p \\ u_t \end{pmatrix}. \qquad (8)$$

One may show that $\boldsymbol{J}_B$, the decoupling matrix for the unicycle-like UAV+camera, is full-rank [3] at the set-point. Hence, introducing the error vector $\boldsymbol{e} = (\,\boldsymbol{s}\quad \theta_p - \pi/2)^T$, and letting

$$\begin{pmatrix} u_\psi \\ u_p \\ u_t \end{pmatrix} = -\boldsymbol{J}_B^{-1} \left(\boldsymbol{K}\boldsymbol{e} + \boldsymbol{J}_A \begin{pmatrix} v \\ \dot{\phi} \end{pmatrix} \right), \qquad (9)$$

with $\boldsymbol{K}$ a 3×3 positive definite diagonal matrix, we guarantee $\dot{\boldsymbol{e}} = -\boldsymbol{K}\boldsymbol{e}$, i.e., decoupled exponential convergence to the set-point (and hence, to a circular trajectory around the target) for the unicycle-like UAV+camera.

4.2 Backstepping to the original UAV+camera dynamics

The original UAV+camera system (1) does not have direct control of the yaw angle: the latter can only be changed through the roll rate (see the third equation of the model). The idea is therefore to design u_ϕ so as to guarantee that the *actual yaw rate* $\dot{\psi}$ of (1) converges to the *virtual yaw control* u_ψ of (7), as given by the first equation in (9). This can be done using a backstepping technique (Sepulchre et al., 1996). The pan and tilt rates, respectively given by the second and third equation in (9), can instead be directly realized by the original UAV+camera system.

The error dynamics for the original UAV+camera system (1) is (compare with (8))

$$\dot{\boldsymbol{e}} = \begin{pmatrix} \dot{\boldsymbol{s}} \\ \dot{\theta}_p \end{pmatrix} = \boldsymbol{J}_A \begin{pmatrix} v \\ \dot{\phi} \end{pmatrix} + \boldsymbol{J}_B \begin{pmatrix} -\dfrac{g}{v}\tan\phi \\ u_p \\ u_t \end{pmatrix}.$$

Adding and subtracting the term $\boldsymbol{J}_B (\, u_\psi\quad u_p\quad u_t\,)^T$ to the right-hand-side we get

$$\dot{\boldsymbol{e}} = \boldsymbol{J}_A \begin{pmatrix} v \\ \dot{\phi} \end{pmatrix} + \boldsymbol{J}_B \begin{pmatrix} u_\psi \\ u_p \\ u_t \end{pmatrix} + \boldsymbol{J}_B \begin{pmatrix} \xi \\ 0 \\ 0 \end{pmatrix}, \qquad (10)$$

where

$$\xi = -\frac{g}{v}\tan\phi - u_\psi$$

is the mismatch between the actual yaw rate and the virtual yaw control. Its time derivative is

$$\dot{\xi} = -\frac{g}{v}\frac{1}{\cos^2\phi}\,\dot{\phi} - \dot{u}_\psi = -\frac{g}{v}\frac{1}{\cos^2\phi}\,u_\phi - \dot{u}_\psi = w, \quad (11)$$

with w an auxiliary input related to the actual input u_ϕ.

Since $(u_\psi\ u_p\ u_t)^T$ has been chosen as in (9), the sum of the first two terms in the right-hand-side of (10) is equal to $-\boldsymbol{K}\boldsymbol{e}$:

$$\dot{\boldsymbol{e}} = -\boldsymbol{K}\boldsymbol{e} + \xi\,\boldsymbol{J}_{B,1}. \qquad (12)$$

We can now prove the following result.

---

[2] The physical reason behind this singularity is simple: when $\boldsymbol{s} = \boldsymbol{0}$ and $\theta_p = \pi/2$, keeping $\boldsymbol{s}$ at zero requires the compensation of the drift term in (6). However, with the pan angle θ_p fixed at its set-point, such compensation would need instantaneous yaw control, which is not available in the UAV+camera system (1).

[3] It can also be shown that $\boldsymbol{J}_B$ has a singularity when the target is exactly below the UAV center of gravity. However, since the UAV moves with a nonzero speed v, it will automatically drive away from the singularity. This, plus the use of a singularity-robust inverse of $\boldsymbol{J}_B$, will be sufficient to guarantee that the control law (9) is always well defined.

Proposition 1. Choosing the auxiliary input w in (11) as

$$w = -\boldsymbol{e}^T \boldsymbol{J}_{B,1} - k_\xi\,\xi, \qquad k_\xi > 0, \qquad (13)$$

yields exponential convergence of ξ to zero (i.e., of $\dot\psi$ to u_ψ) and of $\boldsymbol{s}$, θ_p to the desired set-point. Hence, the UAV will asymptotically move along the desired circular trajectory.

Proof. Consider the following Lyapunov-like function

$$V = \frac{1}{2}\boldsymbol{e}^T\boldsymbol{e} + \frac{1}{2}\xi^2,$$

whose time derivative along the trajectories of the system is

$$\dot V = \boldsymbol{e}^T\dot{\boldsymbol{e}} + \xi\dot\xi = -\boldsymbol{e}^T\boldsymbol{K}\boldsymbol{e} - k_\xi\xi^2,$$

where we have used eqs. (11), (12) and (13). This implies the thesis. ∎

The actual roll rate u_ϕ is computed from (11) and (13) as

$$u_\phi = \frac{v}{g}\cos^2\phi\,(\boldsymbol{e}^T\boldsymbol{J}_{B,1} + k_\xi\,\xi - \dot u_\psi), \qquad (14)$$

where the signal u_ψ is given by the first equation in (9)

$$u_\psi = -(\boldsymbol{J}_B^{-1}\boldsymbol{K})^1\boldsymbol{e} + \boldsymbol{J}_A^1\begin{pmatrix} v \\ \dot\phi \end{pmatrix}. \qquad (15)$$

The pan and tilt rates are instead directly given by the second and third equation in (9).

Due to the fact that system (1) is not in a strict feedback form (Sepulchre et al., 1996), there are in principle two problems when implementing the control law (14–15) for the roll rate. In fact, differentiating u_ψ and plugging the result into (14) both $\dot\phi$ and $\ddot\phi$ appear in the right-hand-side. Hence, an algebraic loop arises; moreover, the control law is non-causal. The first problem can be solved by using a small time delay T equal to the sampling time, i.e., using the last available sample $u_\phi(t - T)$ for $\dot\phi(t)$. Causality is then recovered by replacing $\ddot\phi(t)$ with its *dirty derivative*, computed by stable numerical filtering of $u_\phi = \dot\phi$. Clearly, these approximations are only relevant during the transient phase, as $\dot\phi$ and $\ddot\phi$ are both zero at steady-state.

5. PRELIMINARY SIMULATION

Preliminary simulation of our visual loitering scheme has been performed in MATLAB. The UAV+camera system obeys the dynamics (1), with $z = 10$ m and $v = 10$ m/s; a pinhole camera model is used for image formation.

A typical simulation is the following. With the target fixed w.l.o.g. at the origin of the ground frame, the UAV starts from

$$(x_0, y_0, \psi_0, \phi_0, \theta_{p0}, \theta_{t0}) = (20, -10, \tfrac{3}{2}\pi, 0, \tfrac{2}{3}\pi, -\tfrac{\pi}{4})$$

and moves under the action of the control law (14–15) with gains $\boldsymbol{K} = \mathrm{diag}\{0.5, 0.5, 10\}$ and $k_\xi = 1$. The results are shown in Fig. 4. The top-left plot shows the UAV (triangle) trajectory seen from above, with the crosshair showing the position of the target. As expected, the UAV achieves the desired loitering behavior. The exponential convergence of $\boldsymbol{s}$ and θ_p to their set-point is shown in the top-right and bottom-left plots, respectively, whereas the bottom-right plot confirms that the actual yaw rate $\dot\psi$ of the UAV converges to the virtual yaw control u_ψ of the unicycle-like UAV thanks to the backstepping procedure.
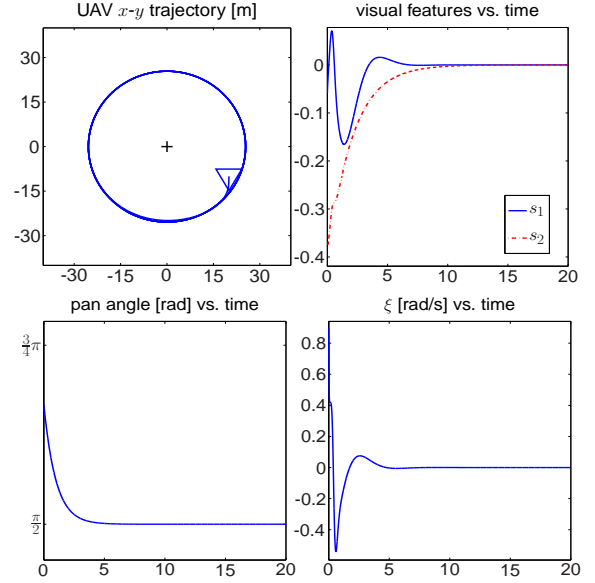

Fig. 4. Basic visual loitering: Simulation on model (1).

6. ENHANCEMENTS TO THE BASIC SCHEME

The simulation results of the previous section confirm the effectiveness of our loitering scheme. However, some further improvements are possible.

6.1 Enforcing a desired radius

The radius of the circular trajectory to which the UAV converges under control (14–15) changes with the initial condition of the system. The possibility of enforcing a desired radius may be welcome in practice. To this end, consider that if the steady-state trajectory is circular then its radius is given by $\rho_\infty = v/\dot\psi_\infty$. Hence, one may impose a desired radius ρ_d by achieving an asymptotic yaw rate

$$\dot\psi_d = \frac{v}{\rho_d}.$$

The idea is therefore to inject this term as a feedforward command in the virtual yaw control u_ψ of the unicycle-like UAV+camera model. To make room for this additional task, we modify our control approach in a *task-priority* sense (Chiaverini et al., 2009) as follows:

$$\begin{pmatrix} u_\psi \\ u_p \\ u_t \end{pmatrix} = -(\boldsymbol{J}_B^{1-2})^\dagger\left(\boldsymbol{K}_s\boldsymbol{s} + \boldsymbol{J}_A^{1-2}\begin{pmatrix} v \\ \dot\phi \end{pmatrix}\right) + \boldsymbol{P}\begin{pmatrix} \dot\psi_d \\ k_p\left(\frac{\pi}{2} - \theta_p\right) \\ 0 \end{pmatrix}$$
$$(16)$$

where $(\boldsymbol{J}_B^{1-2})^\dagger$ is the pseudoinverse matrix of $\boldsymbol{J}_B^{1-2}$, $\boldsymbol{P} = (\boldsymbol{I} - (\boldsymbol{J}_B^{1-2})^\dagger\boldsymbol{J}_B^{1-2})$ is the orthogonal projection matrix in its null space, $\boldsymbol{K}_s$ is a 2×2 positive definite diagonal matrix, and $k_p > 0$. Compared with (9), the modified control law (16) considers only the visual features $\boldsymbol{s}$ as a primary task to be regulated to zero, whereas the secondary task (leading the pan angle to $\pi/2$ and the yaw rate to the desired constant value) is executed as accurately as possible without disturbing the primary. In other words, by this approach we have artificially introduced a single degree of redundancy in the system, which is exploited to achieve a combined secondary task.
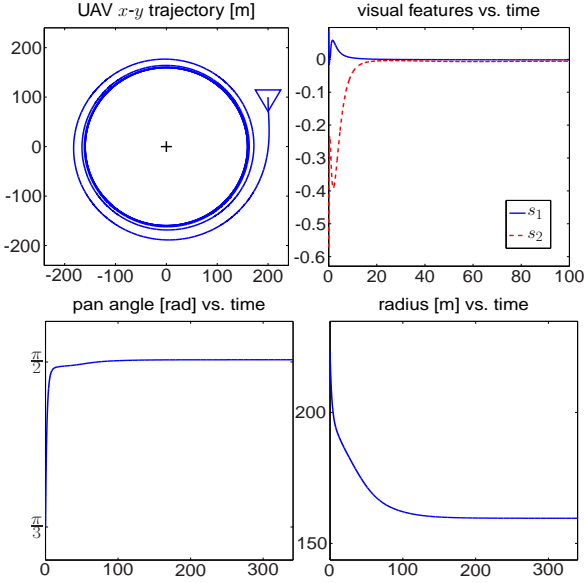
Fig. 5. Enhanced visual loitering: Simulation on an Aerosonde UAV.

Fig. 6. Enhanced visual loitering: Simulation on an Aerosonde UAV in the presence of image noise and wind.

6.2 An alternative to backstepping: Linear roll control

A computationally simpler alternative to the roll rate controller (14) based on backstepping is the following. At each time instant, the virtual yaw control u_ψ, given by the first equation of (9) (or of (16) if a specific radius is enforced), is converted to a current desired value $\bar{\phi}$ for the roll angle using the following formula

$$\bar{\phi} = \arctan\left(-u_\psi \frac{v}{g}\right), \qquad (17)$$

which is directly derived from the third equation of model (1). The roll rate can then be generated via a low-level linear control loop

$$u_\phi = k_\phi(\bar{\phi} - \phi), \qquad k_\phi > 0. \qquad (18)$$

6.3 Estimating the target depth

The above visual loitering method (in all its versions) needs the feature depth Z for computing the interaction matrix $\boldsymbol{J}_i$ in (2). In principle, Z could be computed from the configuration of the UAV+camera system, including the UAV coordinates, and the coordinates of the target. This is in fact the method used in the previous simulations. However, our control approach has been to avoid altogether the use of inertial information. An effective solution is to estimate Z from the evolution of the visual features during the motion. To this end, one can directly use the nonlinear observer proposed by De Luca et al. (2008).

7. SIMULATION ON AN AEROSONDE UAV

Simulations of the modifications of the last section (radius enforcing, linear roll control, depth estimation) on the ideal model (1) confirm that each of them is effective. They are omitted here for lack of space but available at http://www.dis.uniroma1.it/~labrob/research/FWIBVS.html.

In this section, we present a realistic simulation which shows the performance of our visual hovering method (in-cluding all three modifications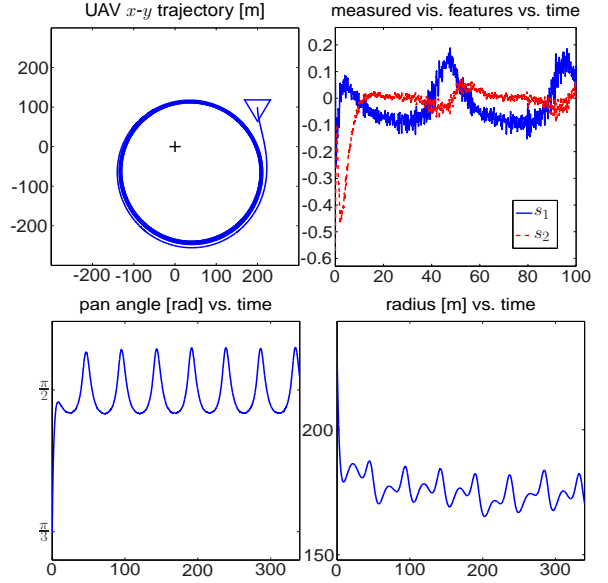 above) on a more complete UAV model. In particular, we have used the simulator of the Aerosonde UAV (http://www.aerosonde.com) included in the Aerosim Blockset by Unmanned Dynamics LLC. To this accurate simulator, which includes aerodynamic effects, we have added low level control loops aimed at improving the adherence of the model to the assumptions of Sect. 2. In particular, airspeed and altitude hold control modes have been implemented via the control of elevator and throttle. The roll rate reference u_ϕ produced by the loitering controller is tracked using a linear control loop on the ailerons, while the rudder is used to achieve coordinated turn with sideslip angle close to zero.

The simulation starts from the initial conditions

$$(x_0, y_0, z_0, \psi_0, \phi_0, \theta_{p0}, \theta_{t0}) = (200, 100, 100, \frac{3}{2}\pi, 0, \frac{\pi}{3}, -\frac{\pi}{4}),$$

with a reference airspeed $v = 25$ m/sec and a feedforward yaw rate $\dot{\psi}_d$ in (16) of 0.15 rad/sec, corresponding to a desired loitering radius of 166.6 m. The target feature depth Z is estimated through the previously mentioned nonlinear observer. The results are shown in Fig. 5.

Even for this realistic model, the visual features converge to zero and the UAV asymptotically loiters on a circular trajectory above the target. Both the pan angle and the loitering radius exhibit a small steady-state error with respect to the desired values (respectively 0.5% and 4%). This mismatch is mainly due to the sideslip and pitch angles being (small but) not zero at steady state. In particular, the nonzero pitch angle is needed to fly at the desired airspeed in view of the realistic simulation of the aerodynamics. As a consequence, the steady-state pan angle required to keep the target at the center of the image plane is also slightly different from $\pi/2$.

To test the robustness of the proposed visual loitering method, we have run the same simulation under perturbations. In particular, we add a zero-mean gaussian random

disturbance with 0.01 variance on each visual feature to simulate camera noise. Moreover, a strong constant wind of 8 m/s (about 30% of the aircraft speed) blows along the x axis[4]. The results, reported in Fig. 6, show that the UAV trajectory is slightly deformed and its center is also displaced. The loitering behavior is however guaranteed together with visual target tracking.

We consider these results to be encouraging given the accuracy of the UAV simulated model. In addition, we have obtained equivalent results when the target is slowly moving. Clips from all simulations are available at `http://www.dis.uniroma1.it/~labrob/research/FWIBVS.html`.

8. CONCLUSIONS

We have presented a control method for driving a UAV equipped with a gimbaled camera to a circular trajectory centered above a ground target using only visual and proprioceptive data. To this end, we have used an IBVS-like approach. In particular, it was first shown that regulation of the visual features plus the pan angle to a suitable set-point entails convergence to the desired kind of trajectory; then, such regulation was achieved for a simplified model of the UAV+camera with direct yaw control; and finally, the same behavior was obtained for the original UAV+camera system through backstepping. Improvements to this basic scheme are possible, including the enforcement of a desired radius for the circular trajectory, a simplified roll control technique, and the integration of a visual depth estimator to make sure that the relative position of the camera w.r.t. the target is not needed for implementation. Simulation results, both for the ideal model and a more realistic case, have been presented to illustrate the performance and robustness of the proposed loitering method.

Future work will address several points, such as maintaining the target in the camera field of view. With the control law (9), a decoupled exponential convergence of $\boldsymbol{s}$ is obtained for the unicycle-like UAV+camera, thus guaranteeing that the target will never leave the field of view during the transient. The same is true for the modified control law (16). However, this does not necessarily hold for the actual UAV+camera system, whose actual yaw rate $\dot{\psi}$ is different from u_ψ during the transient phase. While we never experienced target view loss in simulations, it would be desirable to introduce this constraint explicitly in the backstepping design. We are also planning to implement the proposed method on an actual RC-sized aircraft to perform a more accurate assessment of its robustness.

REFERENCES

Bourquardez, O., Mahony, R., Guenard, N., Chaumette, F., Hamel, T., and Eck, L. (2009). Image-based visual servo control of the translation kinematics of a quadrotor aerial vehicle. *IEEE Trans. on Robotics*, 25(3), 743–749.

Chaumette, F. and Hutchinson, S. (2006). Visual servo control, Part I: Basic approaches. *IEEE Robotics and Automation Mag.*, 13(4), 82–90.

Chen, J. and Dawson, D. (2006). UAV tracking with a monocular camera. In *45th IEEE Conf. on Decision and Control*, 3873–3878.

Chiaverini, S., Oriolo, G., and Walker, I. (2009). Chapter 11: Kinematically redundant manipulators. In O. Khatib and B. Siciliano (eds.), *Handbook of Robotics*, 245–268. Springer.

De Luca, A., Oriolo, G., and Robuffo Giordano, P. (2008). Feature depth observation for image-based visual servoing: Theory and experiments. *The Int. J. of Robotics Research*, 27(10), 1093–1116.

Ding, X.C., Rahmani, A., and Egerstedt, M. (2010). Multi-UAV convoy protection: An optimal approach to path planning and coordination. *IEEE Trans. on Robotics*, 26(2), 256–268.

Drummond, T. and Cipolla, R. (2002). Real-time visual tracking of complex structures. *IEEE Trans. on Pattern Analysis and Machine Intelligence*, 24(7), 932 –946.

Jung, D. and Tsiotras, P. (2008). Bank-to-turn control for a small UAV using backstepping and parameter adaptation. In *17th IFAC World Congress*, 4406–4411.

Le Bras, F., Hamel, T., and Mahony, R. (2009). Image-based visual servo control for circular trajectories for a fixed-wing aircraft. In *48th IEEE Conf. on Decision and Control*, 3430–3435.

Ma, L., Cao, C., Hovakimyan, N., Dobrokhodov, V., and Kaminer, I. (2010). Adaptive vision-based guidance law with guaranteed performance bounds. *Journal of Guidance, Control, and Dynamics*, 33(3), 834–852.

Ponda, S. and Frazzoli, E. (2009). Trajectory optimization for target localization using small unmanned aerial vehicles. In *AIAA Guidance, Navigation, and Control Conf.*

Quigleyand, M., Goodrich, M.A., Griffiths, S., Eldredge, A., and Beard, R.W. (2005). Target acquisition, localization, and surveillance using a fixed-wing mini-UAV and gimbaled camera. In *2005 IEEE Int. Conf. on Robotics and Automation*, 2600–2605.

Regina, N. and Zanzi, M. (2011). UAV guidance law for ground-based target trajectory tracking and loitering. In *2011 IEEE Aerospace Conference*, 1–9.

Roskam, J. (2003). *Airplane Flight Dynamics and Automatic Flight Controls, Part II*. DARcorporation.

Sepulchre, R., Janković, M., and Kokotović, P. (1996). *Constructive Nonlinear Control*. Springer.

Stolle, S. and Rysdyk, R. (2003). Flight path following guidance for unmanned air vehicles with pan-tilt camera for target observation. In *22nd Digital Avionics Systems Conference*, volume 2, 8.B.3.1–12.

Theodorakopoulos, P. and Lacroix, S. (2008). A strategy for tracking a ground target with a UAV. In *2008 IEEE/RSJ Int. Conf. on Intelligent Robots and Systems*, 1254–1259.

Watanabe, Y., Fabiani, P., and Le Besnerais, G. (2009). Simultaneous visual target tracking and navigation in a GPS-denied environment. In *14th Int. Conf. on Advanced Robotics*, 1–6.

---

[4] The perturbation introduced by the wind is actually twofold. First, it acts on the UAV disturbing its motion. Second, the airspeed measured by the on-board sensors is different from the actual ground speed, and this means that the controller uses the former in place of the (correct) latter.